Proc. Natl. Acad. Sci. USA
Vol. 95, pp. 4108–4112, April 1998
Chemistry

Mapping strain exerted on blood vessel walls using deuterium double-quantum-filtered MRI

YEHUDA SHARF*, YOSHITERU SEO†‡, UZI ELIAV§, SOLANG AKSELROD*, AND GIL NAVON§¶

Schools of *Physics and §Chemistry, Tel Aviv University, Tel Aviv, 69978 Israel; and †National Institute of Physiological Studies, Okazaki, 444 Japan

Communicated by Alexander Pines, University of California, Berkeley, CA, November 11, 1997 (received for review August 4, 1997)

ABSTRACT **A technique is described for displaying distinct tissue layers of large blood vessel walls as well as measuring their mechanical strain. The technique is based on deuterium double-quantum-filtered (DQF) spectroscopic imaging. The effectiveness of the double-quantum filtration in suppressing the signal of bulk water is demonstrated on a phantom consisting of rat tail tendon fibers. Only intrafibrillar water is displayed, excluding all other signals of water molecules that reorient isotropically. One- and two-dimensional spectroscopic imaging of bovine aorta and coronary arteries show the characteristic DQF spectrum of each of the tissue layers. This property is used to obtain separate images of the outer layer, the tunica adventitia, or the intermediate layer, the tunica media, or both. To visualize the effect of elongation, the average residual quadrupole splitting $<\Delta\nu_q>$ is calculated for each pixel. Two-dimensional deuterium quadrupolar splitting images are obtained for a fully relaxed and a 55% elongated sample of bovine coronary artery. These images indicate that the strong effect of strain is associated with water molecules in the tunica adventitia whereas the DQF NMR signal of water in the tunica media is apparently strain-insensitive. After appropriate calibration, these average quadrupolar splitting images can be interpreted as strain maps.**

The mechanical properties of blood vessel walls play a central roll in cardiovascular function. At normal blood pressure the length of the vessel is as much as 40% longer and its circumference is about 30% greater than in the unstressed condition. Standard MRI scanning techniques, such as magnetic resonance angiography, provide information about the content of the blood vessels—the blood. But the major site of cardiovascular diseases is in the artery walls. Thus there is a real need to search for new imaging methods able to focus on the blood vessel wall and capable of estimating its biochemical as well as its mechanical conditions. In the present study, we introduce a spectroscopic MRI method for displaying distinct tissue layers of the blood vessel wall as well as measuring its mechanical strain.

To distinguish between the tissue and its surroundings, the measuring technique should be based on some unique property specific to the blood vessel wall. As the tissue consists of various fibrous proteins, collagen, elastin and muscles, a plausible technique would involve the imaging of the protons of the proteins backbone. However, the rigidity of the fibers renders this approach impractical. A more promising approach is to monitor the highly abundant water molecules to explore chemical and structural changes inside the tissue. This approach is reasonable because the NMR relaxation of water molecules signal is chiefly determined by their coupling with the structural elements of the tissue. However, the strong signal of the highly abundant water molecules not associated with the blood vessel walls greatly reduces the dynamic contrast range.

Double-quantum filtering provides an elegant method to suppress the unwanted contribution of bulk water. For spin $I = 1$ nuclei, double-quantum coherences can be formed only in the presence of nonvanishing quadrupolar interaction. Therefore, in the case of ^{2}H NMR of isotropically rotating water molecules, where the ^{2}H quadrupolar interaction averages to zero, no signal is observed after double-quantum filtration (1). In other words the observation of ^{2}H double-quantum-filtered (DQF) NMR signal is indicative for the presence of anisotropic motion.

The blood vessel wall is composed of three layers: the outer layer (the tunica adventitia), the intermediate layer (the tunica media), and the inner layer (the tunica intima). In large arteries the adventitia and the media are very much developed and constitute most of the tissue. Recently we have reported the observation of deuterium DQF NMR signal of water in various large blood vessels. This finding indicated the presence of anisotropic motion of the water molecules, which later was shown to be caused by their interaction with the collagen fibers (2). Furthermore, the deuterium DQF NMR spectrum was found to be highly sensitive to the composition of tissue layers as well as to the strain exerted on the vessel wall (3). Our *in vitro* measurements of bovine carotid and coronary arteries indicated that the ^{2}H DQF NMR spectrum of the tunica media is insensitive to strain and is characterized by a relatively narrow signal and long relaxation times. On the other hand the spectral lineshape of the outer layer, the tunica adventitia, is much broader and is highly sensitive to strain. Thus an imaging method based on ^{2}H DQF NMR can provide a map of both tissue composition and strain distribution within the blood vessel walls.

THEORETICAL BACKGROUND

In a magnetic field, nuclei with spin $I = 1$ have three energy levels, $m_I = 1, 0, -1$. The presence of a nonvanishing quadruplar interaction removes the degeneracy of the two single-quantum transitions, i.e., $|\Delta m_I| = 1$. The "selection rules" of NMR forbid a direct observation of $\Delta m_I \neq 1$. Yet, double-quantum coherences, associated with the transitions $|\Delta m_I| = 2$ between $m_I = 1$ and $m_I = -1$, can be observed indirectly by a sequence of at least three nonselective radio frequency pulses (4, 5). In the DQF NMR experiment only signals that are formed via a period of double-quantum coherences are detected. Thus, for spin $I = 1$ the observation of DQF signal is indicative of the presence of anisotropic motion.

The publication costs of this article were defrayed in part by page charge payment. This article must therefore be hereby marked "*advertisement*" in accordance with 18 U.S.C. §1734 solely to indicate this fact.

Abbreviations: DQF, double-quantum filtered; SI, spectroscopic imaging; GE, gradient echo; 1D, one-dimensional; 2D, two-dimensional; FID, free induction decay; TE, time to echo; TR, repetition time.

‡Present address: Department of Physiology, Kyoto Prefectural University of Medicine, Kamigyo-ku, Kyoto, 602 Japan.
¶To whom reprint requests should be addressed. e-mail: navon@post.tau.ac.il.

The deuterium DQF NMR spectrum of blood vessels immersed in D_2O represents the sum of spectra from many anisotropic compartments. Each compartment can be effectively characterized by a local residual quadrupolar interaction, ω_q, an orientation of the local symmetry axis relative to the external field, θ, and a transverse relaxation rate, R_2. The angular dependency of the observed residual quadrupolar interaction $\omega_{q,\theta}$ is given by

$$\omega_{q,\theta} = \omega_q \frac{1}{2}(3\cos^2\theta - 1). \quad [1]$$

It is convenient to define $P_q(\omega_{q,\theta})$ as the probability density function of finding an anisotropic site with $\omega_{q,\theta}$. $P_q(\omega_{q,\theta})$ is a non-negative function ($P_q(\omega_{q,\theta}) \geq 0$) and $\int_{-\infty}^{\infty} P_q(\omega_{q,\theta})d\omega_{q,\theta} = 1$. The DQF free induction decay (FID) signal is given by ref. 1.

$$\mathrm{FID}(\tau, t) = M_0 \int_{-\infty}^{\infty} P_q(\omega_{q,\theta})\sin(\omega_{q,\theta}\tau)\sin(\omega_{q,\theta}t) \times \exp[-R_2(\tau + t)]d\omega_{q,\theta}, \quad [2]$$

where M_0 is the total magnetization at thermal equilibrium arising from all anisotropic sites. In the derivation of last expression it was assumed that R_2 is constant and that $\omega_{q,\theta} > R_2$ throughout the sample. The latter condition is satisfied for all of the samples of blood vessel walls that we have encountered so far (3). One may note that this assumption does not hold for local directors pointing near the magic angle of $\theta_c = 54.7°$, where according to Eq. **1**, $\omega_{q,\theta}$ vanishes. However, the walls of blood vessels exhibit a broad distribution of local directors, and the relative signal intensities of those local directors near the magic angle is relatively small and therefore may be neglected.

If a creation time $\tau = \tau_0$ is selected to satisfy the condition that $\max(|\omega_{q,\theta}\tau_0|) \ll \pi/2$, the integration of the FID over the acquisition time t, is in the first-order order approximation independent of ω_q and equals

$$I_{\mathrm{FID}} = \int_0^{\infty} \mathrm{FID}(\tau_0, t)dt \approx \tau_0 M_0. \quad [3]$$

Equivalently I_{FID} is given by the intensity of magnitude calculation at the center of the spectrum.

The DQF spectrum, $S(\omega)$, is the Fourier transform of the FID signal in respect to t. Following the above assumptions, i.e., $\max(|\omega_{q,\theta}\tau_0|) \ll \pi/2$ and $|\omega_{q,\theta}| \gg R$. Its imaginary part is given in first-order approximation by

$$\mathrm{Im}\{S(\omega)\} = \frac{-\pi}{2} M_0 \int_{-\infty}^{\infty} P_q(\omega_{q,\theta})\omega_{q,\theta}\tau_0 \times [\delta(\omega - \omega_{q,\theta}) - \delta(\omega + \omega_{q,\theta})]d\omega_{q,\theta} = \frac{-\pi}{2}\omega\tau_0 M_0[P_q(\omega) + P_q(-\omega)]. \quad [4]$$

Considering the odd parity of $\mathrm{IM}[S(\omega)]$ in respect to ω it is clear that $\int_{-\infty}^{\infty} \mathrm{IM}[S(\omega)]d\omega = 0$, as expected for the DQF spectrum. However, the integral $I_s \equiv \frac{2}{\pi}\int_{-\infty}^{\infty} \mathrm{sign}(\omega)\mathrm{Im}[S(\omega)]d\omega$, where $\mathrm{sign}(\omega)$ equals 1 for $\omega \geq 0$ and -1 $\omega < 0$, yields a nonzero value. The last integral can be calculated according to

$$I_s = -\tau_0 M_0 \int_{-\infty}^{\infty} \mathrm{sign}(\omega)\omega[P_q(\omega) + P_q(-\omega)]d\omega = -2\tau_0 M_0 \int_{-\infty}^{\infty} |\omega| P_q(\omega)d\omega. \quad [5]$$

I_s weights the distribution density function by the absolute offset frequency and therefore the ratio $-I_s/I_{\mathrm{FID}}$ can be considered as a measure for the average residual quadrupolar splitting $<\Delta\nu_q>$.

MATERIALS AND METHODS

Samples Preparation. Samples of aorta and coronary arteries were removed from freshly slaughtered healthy cows. The removal of the tissues took place at the municipal slaughterhouse under the supervision of the local veterinarian. The adjacent connective tissues of blood vessels were removed carefully and stored in saline solution at 4°C.

A rat tail was dissected from an anesthetized rat (Wistar-Hamamatsu, 250 g). Several bundles of tendon fibers were separated and stored at 4°C.

Before the measurements the samples were thoroughly rinsed in saline solution, wiped, and immersed in 150 mM NaCl in D_2O for at least 24 h at 4°C.

MRI experiments were conducted on a 300-MHz AMX-WB Bruker NMR spectrometer equipped with 200 G/cm gradient unit and an imaging probe tuned for deuterium frequency (46.05 MHz). For the imaging experiments a coronary artery was mounted on a 3.3-mm diameter Teflon rod, by tying the end of the artery to the ends of the rod. The stretching was accomplished by shortening the strings connecting the ends of the artery to the ends of the rod.

DQF MRI. The ^{2}H DQF spectroscopic imaging (SI) method is based on a sequence of three nonselective RF excitations, where spatial information is obtained by using magnetic field gradients during the evolution of double-quantum coherences (Fig. 1). The phase accumulated during the application of magnetic field gradients is $\exp[i\Delta p(\Delta t\gamma G)\cdot r]$ where Δp (=2) is the change in coherence, G is the strength of magnetic field gradients, γ is the gyromagnetic factor, and Δt stands for the duration of applied gradients.

RESULTS

The ^{2}H DQF SI method was tested on a phantom sample composed of rat tail tendon fibers immersed in D_2O (Fig. 2). The rat tail tendon consists of collagen fibers and exhibits a well-resolved quadrupolar splitting of the deuterium NMR spectrum as expected from a macroscopically oriented system (6). This feature allows a convenient assessment of the effectiveness of the double-quantum filtration in suppressing the signal of bulk water. The phantom consisted of four capillaries:

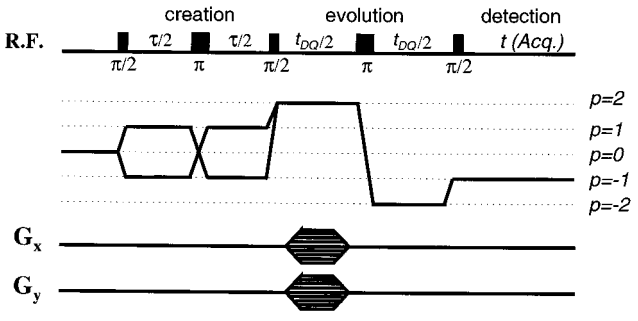

FIG. 1. The DQF MRI experiment.

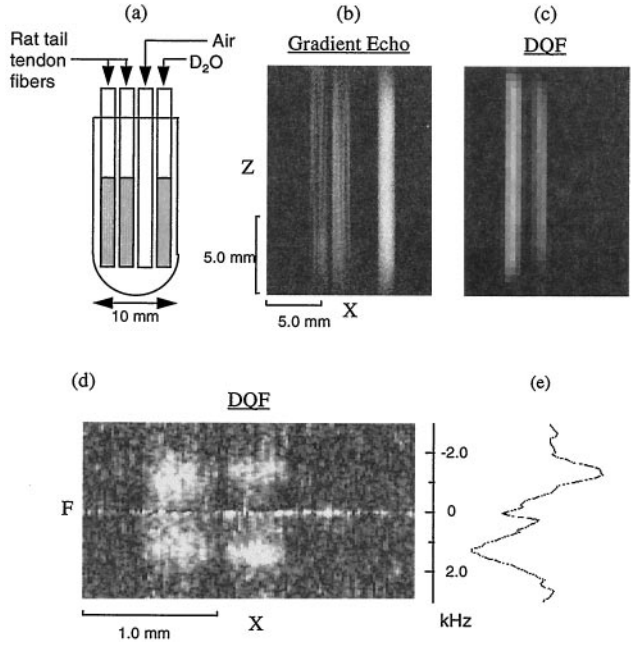

FIG. 2. ^{2}H DQF-SI of rat tail tendon fibers. (*a*) A scheme of the sample. The sample consists of four capillaries (1.2-mm inner diameter): each of the left two contains 5–7 fibers of rat tail tendon immersed in 150 mM NaCl/D_2O, the third from the left is empty, and the rightmost is filled with D_2O. (*b*) ^{2}H GE 2D image of the XZ plane. Field of view is 15 × 15 mm^2, data matrix 128^2, slice thickness 5 mm, repetition time (TR) = 300 ms, time to echo (TE) = 3.3 ms. (c) ^{2}H DQF 2D image at a creation time of 0.2 ms, constructed by projecting the spectroscopic dimension onto the XZ plane. Field of view is 15 × 15 mm^2 × 6.0 kHz, data matrix 32 × 32 × 256, TR = 1 s, DQ evolution time 5 ms. Note that the brighter regions in the GE image (*b*) correspond to the regions containing free D_2O in the spaces between the fibers and in the capillary containing pure D_2O, whereas only intrafibrillar water is apparent in the DQF image (*c*). In *d* a 1D DQF SI of two rat tail tendon fibers (0.5-mm diameter immersed in D_2O in a single capillary acquired with a field gradient strength of 190 G/cm. The *X* and *F* axes stand for the spatial and the spectroscopic dimensions, respectively. (*e*) One of the DQF spectral lines located at the center of the right fibers. The DQF images were acquired with τ = 0.3 ms.

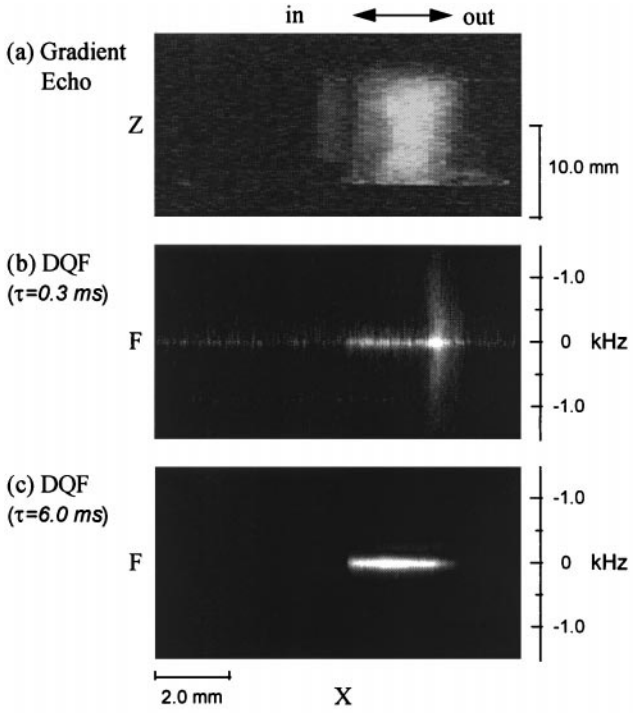

FIG. 3. A 2D ^{2}H GE image and 1D DQF SIs of bovine aorta. The wall of the aorta was cut along the longitudinal axis and a strip of the aorta (12.5 mm in length and 5 mm width) was dissected as a sample. The long and axes of the strip were set in parallel to the *Z* and *Y* axes, respectively. (*a*) 2D ^{2}H GE image of the strip of the aorta in the ZX plane. Field of view 20 × 20 mm^2, data matrix 128^2, slice thickness 8 mm, TR = 200 ms, TE = 5.8 ms. (*b*) 1D DQF spectroscopic image at a creation time of τ = 0.2 ms. Water molecules from all tissue layers contribute to the center (0 kHz) of the spectroscopic axis, whereas only water molecules in the outer layer of the aorta (tunica adventitia) appear in the off-center frequencies. (*c*) 1D DQF spectroscopic image acquired for a creation time of τ = 6.0 ms. At this τ value, the signal from the inner layer (tunica media) reaches its maximum intensity whereas the signal from the outer layer has already decayed. The *X* and *F* represent the axis for the spatial and the frequency dimensions, and their scales are shown in the bottom and the right side of the image, respectively.

two contained fibers of rat tail tendon immersed in D_2O, one was empty, and one was filled with D_2O (see Fig. 2*a*). The image, acquired by using a conventional ^{2}H gradient echo (GE) experiment, was dominated by the strong signal of water in the spaces between the fibers and in the capillary that contained pure D_2O (Fig. 2*b*). This strong signal of isotropically rotating water molecules was completely filtered out in the DQF image (Fig. 2*c*), leaving only contributions from intrafibrillar water molecules that experience anisotropic motion. A one-dimensional (1D) SI of two fibers, taken from the rat tail, is shown in Fig. 2*d*. The relatively high effective spatial resolution of about 40 μm, is achieved by the high field gradient strength. The spectroscopic dimension is preserved as can be seen from the characteristic anti-phased DQF spectral lineshape shown for the right fiber (Fig. 2*e*).

A strip cut of bovine aorta, originally immersed in D_2O, was placed in the NMR tube. The pixel intensity in the conventional ^{2}H GE image is proportional to the total water content, and therefore reflects mostly water in bulk (Fig. 3*a*). Whereas ^{2}H 1D DQF spectroscopic (X-F) images, acquired for various creation times τ, reveals the two distinct tissue layers (Fig. 3 *b* and *c*). For a relatively short creation time (τ = 0.3 ms) all tissue layers contribute to center of the spectrum, whereas the off-center frequency signals ($|\Delta\nu| > 100$ Hz) displays only water in the outer layer with large residual quadrupolar interaction. For a longer creation time (τ = 6.0 ms) the intensity of water in the inner layer increases whereas the signal of water in the outer layer already has decayed. Therefore the center frequency segment represents only the narrow signal of water in the inner layer (practically the tunica media).

These properties were used for obtaining the ^{2}H DQF two-dimensional (2D) histological images of a cross-section of D_2O-hydrated bovine coronary artery shown in Fig. 4. A comparison between the conventional GE image (Fig. 4*a*) and the DQF images (Fig. 4 *b–d*) clearly demonstrates the suppression of the free water signal. Furthermore, the ability of the method to selectively display each of the tissue layers or both allows a convenient measurements of the luminal area as well as the thickness of the layers.

Our uniaxial elongation measurements indicated that the spectrum of water in the outer layer (adventitia) of coronary and carotid arteries is highly sensitive to the strain exerted on the vessel wall; the residual quadrupolar interaction were found to gradually increase with elongation (3). Thus ^{2}H DQF SI may exploit this strain sensitivity to provide a measure of the distribution of the strain throughout the sample.

Two sets of spatially resolved DQF spectra were acquired for a fully relaxed and 55% elongated sample of a bovine coronary artery. To visualize the effect of elongation the average residual quadrupole splitting $<\Delta\nu_q>$ was calculated for each pixel (see *Theoretical Background*). The obtained ^{2}H quadrupolar splitting images are shown in Fig. 5. The color scale

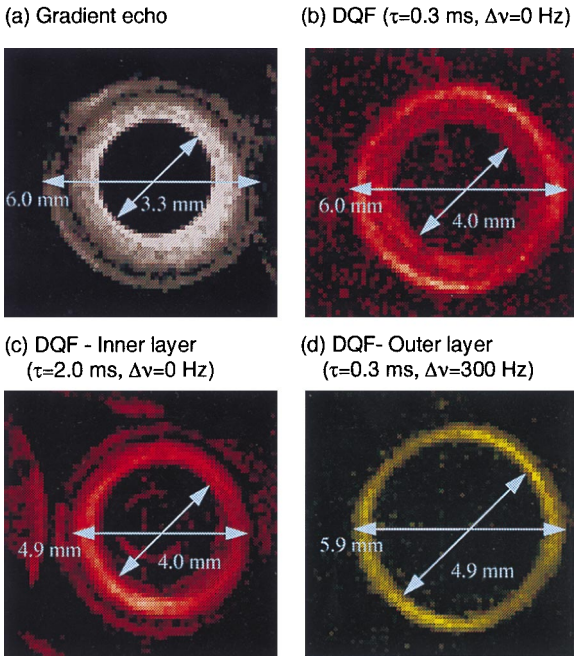

FIG. 4. Histological images of a cross-section bovine coronary artery. A piece of coronary artery (*ca.* 6 mm outer diameter and a length of 12 mm) was equilibrated in D_2O saline. A polyacrilamide rod (3.3-mm diameter) was inserted in the vascular lumen, and both ends of the artery were tied with silk threads.The axis of the artery was set parallel to the magnetic field. (*a*) A 2D ^{2}H GE image of the artery. The image mostly corresponds to the free water in the space between the rod and the tissue, which remained to prevent magnetic susceptibility artifacts. Field of view 10 × 10 mm^2, data matrix 128^2, slice thickness 10 mm, TR = 200 ms, TE = 3.3 ms. (*b–d*) 2D ^{2}H DQF spectroscopic images constructed for a width of 100 Hz in the spectroscopic dimension. The use of different colors (red for ν = 0 Hz and yellow for ν = 300 Hz) emphasizes the fact that the images were taken from different frequency regions. (*b*) 2D 2H DQF SI image measured at τ = 0.3 ms and frequency of 0 Hz in the spectroscopic dimension. The image consists of water in all layers of artery, but water in the lumen is completely suppressed. (*c*) 2D 2H DQF SI image measured at τ = 2.0 ms and ν = 0 Hz in the spectroscopic dimension. Only the water in the inner layer (tunica media) is depicted, and the thickness of the inner layer is 0.9 mm. (*d*) 2D 2H DQF SI image measured at τ = 0.3 ms and ν = 300 Hz in the spectroscopic dimension. Only the water in the outer layer (tunica adventitia) is depicted, and the thickness of the layer is 1.0 mm. Parameters used for 2D ^{2}H DQF SI are as follows: field of view 7.5 × 7.5 mm^2 × 6.0 kHz, data matrix 52 × 52 × 256, TR = 1 s.

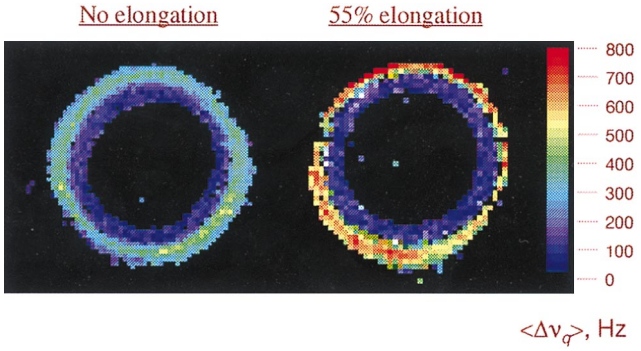

FIG. 5. Two images that display a 2D map of the average ^{2}H quadrupolar splitting, $<\Delta\nu_q>$, of a bovine coronary artery, unstressed (*Left*) and 55% elongated (*Right*). In the magnet the artery, originally equilibrated in D_2O, was aligned with the external magnetic field. $<\Delta\nu_q>$ was calculated by using 256 spectral points for each of the (64 × 64) pixels of the ^{2}H DQF spectroscopic data sets. The left image was acquired by using TR = 1 s, τ = 0.3 ms. To optimize the signal-to-noise ratio for both tissue layers, the right image was calculated by combining two sets of data: for the outer layer, data were acquired by using TR = 0.1 s and τ = 0.3 ms, and for the inner layer, data were acquired by using TR = 0.1 s, τ = 2.0 ms. The field of view of both images was 0.75 cm.

corresponds to $<\Delta\nu_q>$ ranging from 0 to 800 Hz. The bluish colors in both images demonstrate the relatively narrow spectrum of the tunica media, which is insensitive to strain. The cyan-greenish colors that dominate the outer layer, the tunica adventitia, in the left image correspond to $<\Delta\nu_q>$ values of 350–450 Hz for the unstressed vessel. In the right image the yellow-red colors reflect larger values of residual quadrupolar interaction ($<\Delta\nu_q>$ ranges between 550 and 800 Hz) associated with regions with higher strain. The outer layer of the stretched sample exhibits a variety of red and yellow colors. Apparently, this broad distribution of $<\Delta\nu_q>$ is caused by the nonuniform elongation of the sample. It is clear that once $<\Delta\nu_q>$ is appropriately calibrated vs. the elongation, these images can be interpreted as strain maps.

DISCUSSION

The signal observed in the ^{2}H DQF experiment stems solely from intrafibrillar water molecules that interact with the collagen fibers. In fact, collagen is found in all morphological layers of the blood vessel wall. This feature allows a convenient way for determining the boundaries of the vessels wall as well as its infrastructure. Many pathologies, such as atherosclerosis and aneurysm, are well known to be strongly related to the vessel's structure at the location of the malformation. In conventional angiographic methods such deformations are observed indirectly via irregularities in lumen width or in blood flow, for instance as the result of stenosis. Abnormalities in the blood flow pattern tend to occur at a later stage of damage, sometimes long after the process has become irreversible. The capability of the proposed DQF method to display the morphology of the vessel, in particular of the tunica media where most of the interesting pathologies take place, may possibly be used for the earlier detection of morphological changes. For example, such ultrastructural alteration of collagen fibrils in blood vessels were reported during intimal proliferation in rabbit venous aneurysms and atherosclerotic human arteries (7). Moreover, the earlier stages of some pathologies are expressed in gradual changes in the various constituents of the blood vessel wall, i.e., collagen fibers, elastin filaments, muscle tissue, and proteoglycans, as well as in the water content. Our previous results suggested that a change in one of these components causes modification in the collagen network, which then is expressed in the ^{2}H DQF NMR lineshapes through alteration either in the local residual interaction or in the relaxation time (2). The relation between the variations in spectral lineshapes and the clinical state of the tissue is beyond the scope of the present study and needs to be further elucidated. However, such insight should be of important clinical value, providing information about the early onset of vessel disease.

During the cardiac cycle the volume capacity of the vascular system is adjusted to achieve the desired blood pressure. The compliance and resistance of the blood vessel wall are determined by its elastic properties. The present study demonstrates how ^{2}H DQF MRI can be used to create maps of the local strain exerted on the blood vessel wall. The comparison between images of the unstressed bovine coronary artery and the 55% elongated vessel reveals that the effect of strain on the ^{2}H DQF spectra is located in the outer layer, the tunica adventitia. This conclusion stands in good agreement with our previous ^{2}H DQF NMR spectroscopic measurements of carotid and coronary arteries, where the residual quadrupolar interaction of water in the outer layer was found to gradually increase with elongation (3).

Mapping strain using ^{2}H DQF MRI is not restricted to the study of blood vessels. The orientational order in strained elastomers has been studied by using ^{2}H NMR spectroscopy in 1D (8–10), 2D (11), and multidimensional exchange NMR (12). Recently, the quadrupolar interaction of deuterated poly (butadiene) oligomers incorporated into elastic rubber band was used to generate contrast in ^{2}H DQF MRI of strained elastomers (13, 14). In the present study we have shown how both the magnetization of the anisotropically reorienting spins and the averaged quadrupolar splitting can be evaluated for each pixel without the need of elaborate methods. Moreover, the method used for creating the average quadrupole splitting images provides a convenient means to calibrate data sets acquired from distinct experiments. Thus the ^{2}H DQF MRI can be implemented to yield a quantitative evaluation of the local residual strain in either blood vessel walls or strained elastomers.

Considering the sensitivity of ^{2}H nuclei, the method can be applied for *in vitro* studies of samples enriched with D_2O. However, the relatively low natural abundance of deuterium (0.015%) restricts the feasibility of *in vivo* experiments to small laboratory animals (15). A favorable way to circumvent this restraint is to measure the effect of strain on the proton–proton dipolar interaction. In comparison to quadrupolar nuclei, the advantageous of the ^{1}H nucleus for NMR applications is apparent because of its large gyromagnetic ratio and its high natural abundance in biological tissues. Dipolar interaction is spatially dependent and, similarly to quadrupolar interaction, in the presence of anisotropic motion, it induces a nonzero residual dipolar term in the Hamiltonian. Indeed, experiments performed on several intact tissues exhibited DQF signals of ^{1}H arising from molecules with anisotropic motion (16). Other studies reported the direct measurements of weak proton–proton dipolar interaction in natural rubber, under uniaxial stretching (17).

In conclusion, ^{2}H DQF MRI can yield histological as well as strain images of blood vessels. The method is extremely powerful because: (*i*) unwanted contributions from free water are completely eliminated by the double-quantum filtration; (*ii*) one can easily achieve separate images of distinct tissue layers (either the tunica media or the tunica adventitia or both); and (*iii*) the additional spectroscopic dimension provides quantitative information about the degree of strain. By a proper calibration a strain map of the blood vessel wall might be obtained without the need of elaborated methods.

The work was supported in part by a grant from the German–Israeli Binational Foundation (GIF) to G.N.

1. Sharf, Y., Eliav, U., Shinar, H. & Navon, G. (1995) *J. Magn. Reson. B* **107,** 60–67.
2. Sharf, Y., Knubovets, T., Dayan, D., Hirshberg, A., Akselrod, S. & Navon, G. (1997) *Biophys. J.* **36,** 1198–1204.
3. Sharf, Y., Akselrod, S. & Navon, G. (1997) *Magn. Reson. Med.* **37,** 69–75.
4. Vega, S., Shattuck, T. W. & Pines, A. (1976) *Phys. Rev. Lett.* **37,** 43–46.
5. Bodenhausen, G., Vold, R. L. & Vold, R. R. (1980) *J. Magn. Reson.* **37** 93–106.
6. Berendsen, H. J. C. (1962) *J. Chem. Phys.* **36,** 3297–3305.
7. Stehbens, W. E. & Martin, B. J. (1993) *Connect. Tiss. Res.* **29,** 319–331.
8. Deloche, B. & Samulski, E. T. (1981) *Macromolecules* **14,** 575–581.
9. Gronski, W., Stadler, R. & Jacobi, M. M. (1981) *Macromolecules* **17,** 741–748.
10. Sotta, P., Deloche, B., Herz, J., Lapp, A., Durand, D. & Rabadeux, J. C. (1987) *Macromolecules* **20,** 2769–2774.
11. Hansen, T., Blumich, B., Boeffel, C. & Spiess, H. W. (1992) *Macromolecules* **25,** 5542–5544.
12. Schaefer, D., Leisen, J. & Spiess, H. W. (1995) *J. Magn. Reson. A* **115,** 60–79.
13. Klinkenberg, M., Blümler, P. & Blümich, B. (1996) *J. Magn. Reson. A* **119,** 197–203.
14. Klinkenberg, M., Blümler, P. & Blümich, B. (1997) *Macromolecules* **30,** 1038–1043.
15. Assaf, Y., Navon, G. & Cohen, Y. (1997) *Magn. Reson. Med.* **37** 197–203.
16. Tsoref, L., Shinar, H. & Navon, G. (1998) *Magn. Reson. Med.* **39,** 11–17.
17. Callaghan, P. T. & Samulski, E. T. (1997) *Macromolecules* **30,** 113–122.